CrossMark

About thermostability of biocompatible Ti–Zr–Ta–Si amorphous alloys

Mircea Nicoara[1] · **Aurel Raduta**[1] · **Cosmin Locovei**[1] · **Dragos Buzdugan**[1] ·
Mihai Stoica[1,2]

Abstract Ti-based amorphous alloys produced by ultra-rapid melt cooling represent an excellent option as biomaterials because of their mechanical properties and corrosion resistance. However, complete elimination of toxic elements is affecting the glass-forming ability and amorphous structure could be obtained only for thin ribbons or powders that are subsequently processed by powder metallurgy. Amorphous ribbons of special $Ti_{42}Zr_{40}Ta_3Si_{15}$ alloy, which is completely free of any toxic element, were produced by melt spinning, and the thermostability of resulting material was investigated in order to estimate its ability for further heat processing. Isochronal differential scanning calorimetry (DSC) was used to determine transformation points such as glass transition temperature T_g or crystallization temperature T_x. The activation energy for crystallization of amorphous phase was calculated based on Kissinger method, using heating rates ranging between 5 and 20 °C min^{-1}. Amorphous structure of resulting ribbon was evidenced by means of X-rays diffraction (XRD) and high-resolution transmission electron microscopy (HR-TEM). It was determined that amorphous $Ti_{42}Zr_{40}Ta_3Si_{15}$ alloy has a high activation energy for crystallization, similar to other Ti-based amorphous alloys, which provides good thermal stability for subsequent processing, especially by means of powder metallurgy techniques.

✉ Mircea Nicoara
mircea.nicoara@upt.ro

1 Politehnica University Timisoara, 300222 Timisoara, Romania

2 Institute for Complex Materials, 01069 Dresden, Germany

Introduction

Titanium alloys represent the most used biomaterials in orthopedics and dentistry, because they combine excellent mechanical properties and corrosion resistance. In spite of extensive use, some important inconveniences still persist. Titanium alloys have high mechanical resistance and suitable ductility, which provide very good loading capacity for orthopedic and dental implants, but they have rigidities higher than human bone. This fact is responsible for the stress shielding effect, which consists in progressive reduction in bone density, culminating sometimes with implant failure. For example, Ti-6Al-4V, which is the most popular titanium alloy for fabrication of orthopedic implants, has Young's modulus around 112 GPa, while cortical bone has rigidity values ranging between 4 and 30 GPa [1–4].

Another important problem related to the use of titanium alloys is biological safety of alloying elements, which are responsible for releasing metallic ions. For example, Ni, which is extensively used as amorphization element for newly developed bulk metallic glasses (BMGs) with titanium base, has been proved to be allergenic, and possible cause for other harmful effect to human body, such as genotoxicity, carcinogenicity, and mutagenicity. Some extensively used amorphization elements with proven cytotoxic effect are Cu, Ag, Zn, and Be. Others such as Co, Cr, Fe, Mo, V, Al, and Mn are responsible for adverse tissue reactions. The large number of alloying elements that are harmful to human body is considerably limiting the development of new titanium-based biomaterials. The design of new compositions is based on a list of alloying additions considered non-problematic, which are eligible for future researches. This list includes Nb, Ta, Zr, Si, Mo, Sn, Pd, In, Sr, B, Ca, and Mg [5–12].

Overcoming the two major drawbacks of existing titanium alloys, i.e., excessive rigidity and toxic effects to human body, attracts considerable interest, and therefore the development of new compositions appears to be promising. Amorphous alloys have no discontinuities such as grain boundaries or dislocations and thus show increased corrosion resistance. Such structures have different deformation mechanisms than crystalline alloys, which provide an interesting combination of high yield strength and lower Young's modulus. A promising alternative to improve the relatively low ductility of BMGs is the BMG composites. They have heterogeneous microstructure, in which the glassy matrix is combined with second phase particles that could be crystalline (pure elements, solid solution, or intermetallics), quasi-crystalline, and even amorphous [13, 14].

One of the most important technological problems to be solved is that existing titanium-based BMGs usually contain harmful elements such as Ni, Cu, Al, or Be, in order to provide sufficient glass-forming ability (GFA) for bulk components. Therefore, newly developed biocompatible alloys containing additions of Zr, Si, Ta, Pd, and Nb are fabricated as thin amorphous ribbons, by means of rapid cooling techniques, such as melt spinning. Resulting biomaterials have better electrochemical stability and excellent biocompatibility response [15–20].

Ribbons could be furtherly processed via powder metallurgy techniques, which usually include milling to amorphous powder and consolidation by means of hot pressing or extrusion. Parameters control during powder metallurgy processing also allows fabrication of bulk amorphous materials with controlled porosity, usually called bulk metallic glass foams (BMGFs) [21]. Fabrication of porous materials by means of powder metallurgy could provide biomechanical compatibility, since resulting porosity reduces the Young's modulus close to rigidity of human bone. Superficial porosity also increases the interface between bone and implant offering better implant fixation. Higher porosity and pore interconnectivity stimulate cell migration and bone growth at better mechanical properties than scaffolds bioactive ceramics [22–25].

One of the most important technological problems during processing of amorphous ribbons by means of powder metallurgy is conservation of amorphous structure along the fabrication route, especially when heating is involved. Therefore, thermostability of new formulated composition should be determined in terms of critical transformation points and activations energy. The aim of the current work is fabrication of fully amorphous $Ti_{42}Zr_{40}Ta_3Si_{15}$ ribbons and evaluation of thermal stability, based on calculation of activation energy for crystallization.

Materials and methods

Experimental

The present experimental program is focused on fabrication of an amorphous $Ti_{42}Zr_{40}Ta_3Si_{15}$ alloy that contains only biocompatible elements, and which is suitable for subsequent processing by means of powder metallurgy. The GFA of considered alloy is too low for casting of BMG components, i.e., having critical dimensions above 1 mm. Therefore, the fabrication route includes casting of thin ribbons by means of melt spinning, which allows amorphization of alloys with low GFA. The ribbons are subsequently milled and resulting powder consolidated by means of hot pressing. Investigations of differential scanning calorimetry (DSC) were performed using samples of about 20 mg under argon gas on a Netzsch differential scanning calorimeter (DSC) in order to determine transformations points and calculate the activation energy. This information is necessary for further optimization of hot pressing parameters, i.e., processing temperature and duration.

The master alloy with atomic composition $Ti_{42}Zr_{40}Ta_3Si_{15}$ was prepared by arc melting in titanium-gettered argon atmosphere. Only high-purity elements (purity 99.9 mass% and better) were used, and, because the components have very diverse melting points, the resulted ingot was melt and flipped repeatedly to provide better homogeneity [26].

Melt spinning was performed on a single-roller Bühler melt spinner with the wheel circumferential speed 35 ms^{-1}. The melt was overheated to $T = 1973$ K and ejected at argon relative pressure of 400 mbar. The resulting ribbons were 5 mm wide and 45 μm thick.

In order to determine the structural state of resulting ribbons, X-rays diffraction (XRD) was performed on an Inel Equinox 1000 high-resolution X-Ray diffractometer with curved detector, using Co radiation, which can measure all diffraction peaks simultaneously.

Amorphous or crystalline character of resulting microstructure was confirmed by means of high-resolution transmission electron microscopy (HR-TEM) using a FEI Tecnai G2 200 kV S/TEM. TEM samples were prepared on FEI Quanta 3D dual beam microscope, using focused beams of gallium ions.

Theoretical considerations

Ribbons fabricated by ultra-rapid cooling are in a metastable state, characterized by a higher internal energy than the stable crystalline state. Consequently, during heating, the amorphous alloys tend to reduce the level of

free energy during the first stage of transformation, while amorphous structure is still preserved, and crystallization occurs during the second stage of transformation. Heating below crystallization point produces reduction in the free energy as result of relaxation processes, which includes short-range structural changes, causing also some changes of physical characteristics, such as specific volume, specific heat, hardness, ductility. Structural changes during second stage of heating involve some polymorphous reactions, which produce crystallization, without any changes of chemical composition. Some amorphous alloys have more complicated crystallizations associated with reactions of decomposition [27].

It is of utmost importance to determine crystallization temperature of amorphous alloys, since large majority of applications require preservation of amorphous structure for stability of properties, throughout subsequent processing and further on during the entire life of components. Alloys compositions that are furtherly processed by means of powder metallurgy must have transformation temperature as high as possible because consolidation of powder involves hot processing, such as sintering, pressing, extrusion.

Crystallization of metallic glasses could be characterized by indicating the formation rate of crystalline germs Q, the crystals growth rate V, and activation energy of crystallization E_a. If isothermal crystallization is considered, parameter Q is determined by using the following relation:

$$Q = Q_0 \times e^{-\frac{N\Delta G_c}{RT}} \times e^{-\frac{E_n}{RT}} \tag{1}$$

The symbols in Eq. (1) have following significations: Q_0—rate on which the grain number increases from 10^{30} to 10^{35} germs cm^3, N—Loschmidt's number, E_n—activation energy necessary to pass an atom over the limits of nucleus, and ΔG_c—amount of free energy required to form nuclei having radii equal to critical radius.

Similarly, Eq. (2) expresses the crystals growth rate:

$$V = V_0 e^{-\frac{Q_q}{RT}}\left(1 - e^{-\frac{\Delta G_C}{RT}}\right) \tag{2}$$

where symbols have following meaning: Q_q—quantity of energy necessary for an atom to leave amorphous state and associate to crystal, ΔG_C—change of free energy during crystallization, V—crystal growth rate, and $V_0 = a_0 \times v_0$, where a_0 is the atomic diameter and v_0, is the atomic jump frequency.

If the temperature level T is much below the melting point T_f of alloys, i.e., there is a very high undercooling, changes of energy $\Delta G_c \gg RT$, Eqs. (1) and (2) can be expressed, respectively, as [28]:

$$V = V_0 e^{-\frac{Q_q}{RT}} \tag{3}$$

and

$$Q = Q_0 e^{-\frac{EQ_n}{RT}} \tag{4}$$

New formulas in Eqs. (3) and (4) indicate that both the growth and crystallization rates could be similarly expressed with the Arrhenius equation.

The activation energy of crystallization E_a [J mol^{-1}] could be calculated following Kissinger's relation [29–34]:

$$ln\left(\frac{T_v^2}{V_i}\right) = \frac{E_a}{RT_v} + A \tag{5}$$

The symbols have the following meanings: T_v [K]—temperature point corresponding to maximum crystallization rate, V_i [K s^{-1}]—heating rate used to determine the DSC curve, R [J mol^{-1} K^{-1}]—universal constant of gases, and A—constant specific to analyzed material [35, 36].

Activation energy for crystallization of certain phase E_a could be determined based on Eq. (5) as the slope of the line represented in following coordinates:

$$ln\left(\frac{T_v^2}{V_i}\right) = F\left(\frac{1}{T_v}\right) \tag{6}$$

Results and discussion

For further investigation, it is crucial to start from a fully amorphous ribbon. Therefore, a special attention was given to the investigation methods, in order to rule out the presence of any (nano) crystalline inclusion. The amorphous nature of the cast ribbons was proved by both XRD and TEM. Figure 1 shows the HR-TEM image of as cast $Ti_{42}Zr_{40}Ta_3Si_{15}$ amorphous ribbons. The electron diffraction (SAED) pattern corresponding to the selected area is presented in the inset, right side of the picture. The left-side inset is the XRD pattern. The HR-TEM micrographs show only the random disordered distribution, which is typical to amorphous structure. The 2D SAED pattern presents also only the amorphous halo, as characteristic to the amorphous structure. Additionally, the XRD performed in Bragg–Brentano configuration did not evidenced any crystalline sharp reflection, as seen in the second inset. Therefore, it can be concluded with no doubts that the cast $Ti_{42}Zr_{40}Ta_3Si_{15}$ ribbons are fully amorphous.

Figure 2 shows the DSC curve measured at a 20 °C min^{-1} constant heating rate. Despite the fact that the $Ti_{42}Zr_{40}Ta_3Si_{15}$ ribbons were proved to be fully amorphous, the glass transition event in the curve is quite weak. Often marginal glass formers do not exhibit a glass transition, at least at conventional heating rates as those used in this work [27]. In fact, the first authors who studied this composition, Lin et al., encountered serious difficulties in

Fig. 1 HR-TEM image of as-cast amorphous ribbons. The *inset* in the *left side* shows the corresponding SAED pattern, while the *inset* in the *right side* is the typical XRD pattern
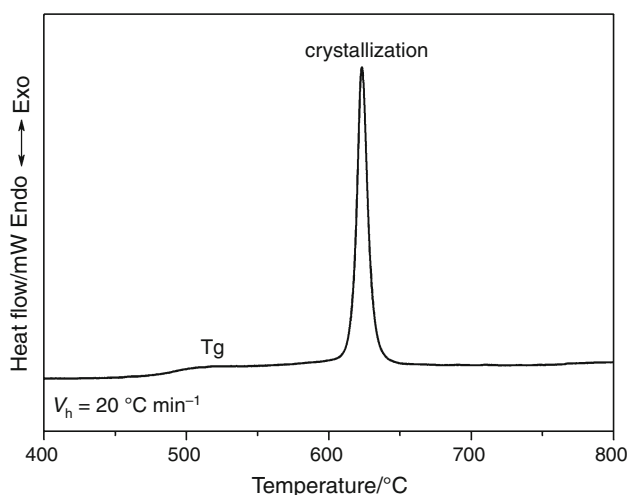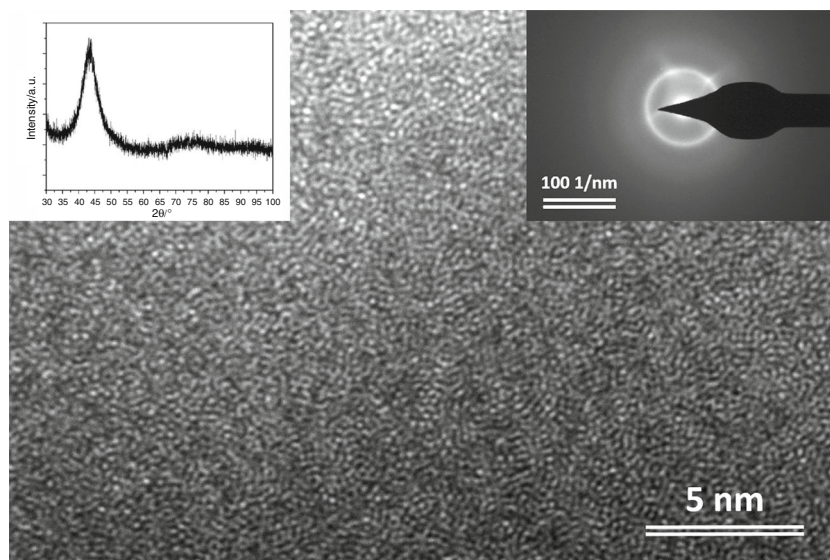

Fig. 2 DSC curve for $Ti_{42}Zr_{40}Ta_3Si_{15}$ amorphous alloy ribbon measured at a constant heating rate of 20 °C min^{-1}
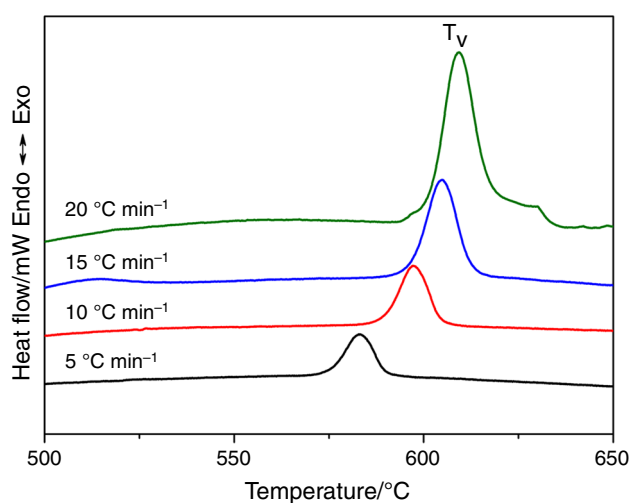

Fig. 3 DSC curves measured at different heating rates. Peak temperatures T_v are considered further for Kissinger analysis

determining correctly the glass transition temperature. In our case, as it is seen in Fig. 2, a small but clear endothermic event associated with the glass transition can be seen. This is in agreement with our previous findings [37]. The glass transition temperature, measured as the onset of this event, is $T_g = 513$ °C. Further, the samples crystallize through a single, sharp exothermic peak, heaving the onset at $T_x = 616$ °C.

Evaluation of stability for amorphous structures is based on the activation energy necessary for crystallization, which is responsible for dramatic alteration of properties. Therefore, the DSC curves were also determined at different heating rates, i.e., 5, 10, 15, and 20 °C min^{-1}. They are presented in Fig. 3. The appearance of the endothermic

event associated with the glass transition is even more faded when the heating rate for isochronal experiment decreases. This is obvious, because the slow heating allows structural relaxation prior crystallization. However, for further analyses, the exothermic peak temperatures are of first importance.

The formation of crystalline entities usually proceeds with different rates, according to the reaction kinetics [27]. The transformation of the amorphous phase into crystalline phase takes place through nucleation and growth. Both events are temperature dependent; therefore, the rates at which they proceed are easily determined upon isothermal experiments. However, in the case of isochronal DSC measurements, the maximum crystallization rate would

correspond to the temperature of the exothermic peak, as marked at T_v in Fig. 3. Table 1 summarizes the experimentally determined temperatures, which further allow the calculation of Kissinger plot as represented in Fig. 4.

The activation energy for crystallization of the $Ti_{42}Zr_{40}Ta_3Si_{15}$ amorphous alloy was determined based on representation in Fig. 4 and is numerically equivalent to the slope of the line. The value is $E_a = 310$ kJ mol^{-1} and is comparable with activation energies determined for similar amorphous alloys. For example, the activation energy of amorphous $Ti_{40}Zr_{10}Cu_{36}Pd_{14}$, which is considered to have high thermal stability of crystallization, determined with Kissinger's method is 287.6 kJ mol^{-1} [38].

Calculations of activation energies for crystallization of different amorphous Ti-based alloys have attracted considerable interest, since higher crystallization stability could facilitate conservation of amorphous character during subsequent thermal processing. Although the method based on Kissinger's plots, calculated from DSC curves that are obtained by isochronal heating at different rates, is considered less accurate, comparative studies on glassy Ti alloys reveal good agreement with isothermal investigations. For comparison, activation energy for crystallization of $Ti_{48}Ni_{32}Cu_8Si_8Sn_4$ BMG is 369.1 kJ mol^{-1} for

Table 1 Parameters of DSC heating curves

No.	Heating rate V_i/°C min^{-1}	Tip of the peak T_v/°C
1	5	583
2	10	597
3	15	605
4	20	609

Fig. 4 Kissinger's line of $Ti_{42}Zr_{40}Ta_3Si_{15}$ amorphous alloy

isochronal heating, calculated after Kissinger, and 381.8 kJ mol^{-1} for isothermal annealing [39].

Non-isothermal methods are extensively used to determine the effect of different alloying elements on thermal stability to crystallization of amorphous alloys. For example, Pratap et al. [40] determined that partial replacement of Cu with Ni in Ti-based amorphous alloys was producing an increase in activation energy, calculated after Kissinger, from 207 kJ mol^{-1} for $Ti_{50}Cu_{50}$ to 406 kJ mol^{-1} in the case of $Ti_{50}Ni_{30}Cu_{20}$. It is worth noting that similar values of activation energies resulted by means of Augis–Bennet or Ozawa methods of calculation. Similarly, the two crystallization reactions of $Ti_{20}Zr_{20}Cu_{60}$ metallic glass, calculated by Kissinger's method, have activation energies of 392 and 320 kJ mol^{-1}, respectively, close to the values resulting from alternative methods (Augis–Bennet, Boswell, Ozawa, Gao-Wang) [41]. Other authors also emphasize that in the case of amorphous alloys, Kissinger's calculations are in good accordance with results obtained by other methods, such as Moynihan or Augis [42]. Another study [43] evidences that the amorphous $Ti_{41.5}Zr_{2.5}Hf_5Cu_{37.5}Ni_{7.5}Si_1Sn_5$ has an activation energy of crystallization of 409.51 kJ mol^{-1} (after Kissinger), and therefore has a higher stability than the corresponding Sn-free alloy, with an activation energy of only 399.84 kJ mol^{-1}. In the case of $Ti_{53}Cu_{27}Ni_{12}Zr_3Al_7Si_3B_1$ BMG, which evidences three distinct crystallization peaks on DSC curves, the activation energies calculated after Kissinger's are 377.86, 322.97, and 311.17 kJ mol^{-1}, respectively, for the three resulting crystalline phases, although their compositions remain partially uncertain [44]. Additional alloying of the same BMG with small quantities of Sc, Hf, Ta, and Nb results in activation energies for primary crystallization of 356.31, 355.02, 437.27, and 375.55 kJ mol^{-1}, respectively, which emphasizes the stabilizing effect of Ta, which significantly increases the activation energy [45]. The effect of different alloying elements on the crystallization stability of Ti–Zr–Be bulk metallic glasses was evaluated also by means of Kissinger's method. The activation energy for basic amorphous $Ti_{41}Zr_{25}Be_{34}$ is 181.3 kJ mol^{-1}, which increases with addition of Cu, Al, Cr, V, and especially Ag that provides the highest activation energy of 242.5 kJ mol^{-1}, while Fe and Ni have the opposite effect. Crystallization of initial $Ti_{41}Zr_{25}Be_{34}$ alloy normally produces α-Ti_2Zr, Be_2Zr, and α-Ti phases, but addition of elements like Fe, V, Cr results in formation of β-Ti, or some unknown phases when Cu and Ni are added [46]. Alloying the $Ti_{41}Zr_{25}Be_{28}Fe_6$ BMG with 7 % at Cu also determines the growth of activation energy of crystallization, determined with the Kissinger method, for the first DSC crystallization peak, from 179 to 188 kJ mol^{-1}. The effect of Cu alloying consists also in some modification of crystallization

kinetics, since the isochronal DSC curve of the basic $Ti_{41}Zr_{25}Be_{28}Fe_6$ alloy has only two exothermic reactions of crystallization, while modified $(Ti_{41}Zr_{25}Be_{28}Fe_6)_{93}Cu_7$ has four such peaks. This effect is considered to reduce the nucleation and growth rate, making atomic diffusion more difficult and therefore increasing the glass-forming ability (GFA) [47].

The Kissinger's method is used also for comparative characterization of amorphous Ti-based powders produced by mechanical alloying from pure elements or mechanical milling of intermetallic compounds. For example, the activation energy for crystallization of $Ti_{60}Cu_{15}Ni_{15}Al_{10}$ amorphous powders is 260.5 and 266.5 5 kJ mol^{-1} if obtained by means of mechanical alloying or mechanical milling, respectively [48]. In conclusion, activation energies for crystallization of amorphous $Ti_{42}Zr_{40}Ta_3Si_{15}$ are situated approximately in the same range with many Ti-based or Zr-based alloys [49, 50] that are considered highly stable against crystallization, but still lower than in the case of Fe-based amorphous alloys [51].

Information about the high activation energy of crystallization that was determined by means of Kissinger's method for amorphous $Ti_{42}Zr_{40}Ta_3Si_{15}$ alloy should be corroborated with isothermal DSC investigations performed on the same alloy by Lin et al. [15]. They determined that incubation time during isothermal annealing range between 3000 at 550 and 1000 s at 580 °C. The combination of high activation energy and relatively long incubation time opens important perspective for subsequent processing of melt spun ribbons into massive components by means of powder metallurgical routes, without affecting the amorphous character.

Conclusions

Despite a reduced glass-forming ability, the results clearly show the possibility to cast fully amorphous ribbons of $Ti_{42}Zr_{40}Ta_3Si_{15}$ alloy that have a high thermal stability. The calculated value of activation energy for crystallization is close to the typical values presented in the literature for similar Ti-based alloys and recommends this new alloy as suitable for processing by means of powder metallurgy, without alterations of amorphous character or relevant properties. Considering the composition, which is completely free of any harmful elements, this new alloy has considerable potential as biomaterial for applications as orthopedic or dental implants.

References

1. Basu B, Katti DS, Kumar A. Advanced biomaterials—fundamentals, processing, and applications. Hoboken: Wiley; 2009.
2. Chen Q, Thouas GA. Metallic implant biomaterials. Mat Sci Eng R. 2015;87:1–57.
3. Abdel-Hady MG, Niinomi M. Biocompatibility of Ti-alloys for long-term implantation. J Mech Behav Biomed Mater. 2013;20:407–15.
4. Qin F, Dan Z, Wang X, Xie G, Inoue A. Ti-based bulk metallic glasses for biomedical applications. In: Laskovski AN, editor. Biomedical Engineering, Trends in Material Science. InTech; 2011.
5. Biesiekierski A, Wang J, Gepreel MA-H, Wen C. A new look at biomedical Ti-based shape memory alloys. Acta Biomater. 2012;8:1661–9.
6. Merritt K. Role of medical materials, both in implant and surface applications, in immune response and in resistance to infection. Biomaterials. 1984;5:47–53.
7. Schlede E, Aberer W, Fuchs T, Gerner I, Lessmann H, Maurer T, Rossbacher R, Stropp G, Wagner E, Kayser D. Chemical substances and contact allergy—244 substances ranked according to allergenic potency. Toxicology. 2003;193:219–59.
8. Elshahawy WM, Watanabe I, Kramer P. In vitro cytotoxicity evaluation of elemental ions released from different prosthodontic materials. Dent Mater. 2009;25:1551–5.
9. Hornez J, Lefevre A, Joly D, Hildebrand H. Multiple parameter cytotoxicity index on dental alloys and pure metals. Biomol Eng. 2002;19:103–17.
10. Kuroda D, Niinomi M, Morinaga M, Kato Y, Yashiro T. Design and mechanical properties of new b type titanium alloys for implant materials. Mat Sci Eng A. 1998;243:244–9.
11. Long M, Rack H. Titanium alloys in total joint replacement—a materials science perspective. Biomaterials. 1998;19:1621–39.
12. Calin M, Gebert A, Ghinea AC, Gostin PF, Abdi S, Mickel C, Eckert J. Designing biocompatible Ti-based metallic glasses for implant applications. Mat Sci Eng C. 2013;33:875–83.
13. Greer AL. Metallic glasses… on the threshold. Mater Today. 2009;12(1–2):14–23.
14. Eckert J, Das J, Pauly S, Duhamel C. Mechanical properties of bulk metallic glasses and composites. J Mater Res. 2007;22(2):285–301.
15. Lin H, Tsai P, Ke J, Li J, Jang J, Huang C, Haung J. Designing a toxic-element-free Ti-based amorphous alloy with remarkable supercooled liquid region for biomedical application. Intermetallics. 2014;55:22–7.
16. Abdi S, Khoshkhoo MS, Shuleshova O, Bönisch M, Calin M, Baró M, Sort J, Gebert A. Effect of Nb addition on microstructure evolution and nanomechanical properties of a glass-forming TiZrSi alloy. Intermetallics. 2014;46:156–63.
17. Oak JJ, Inoue A. Formation, mechanical properties and corrosion resistance of Ti–Pd base glassy alloys. J of Non-Crys Solids. 2008;354:1828–32.
18. Oak JJ, Inoue A. Attempt to develop Ti-based amorphous alloys for biomaterials. Mat Sci Eng A. 2007;449–451:220–4.
19. Ke J, Huang C, Chen Y, Tsai W, Wei T, Huang J. In vitro biocompatibility response of Ti–Zr–Si thin film metallic glasses. Appl Surf Sci. 2014;322:41–6.
20. Lin C, Huang C, Chuang J, Huang J, Jang J, Chen C. Rapid screening of potential metallic glasses for biomedical applications. Mat Sci Eng C. 2013;33:4520–6.

21. Li J, Lin H, Jang JKC, Huang J. Novel open-cell bulk metallic glass foams with promising characteristics. Mat Lett. 2013;105:140–3.

22. Zhuravleva K, Chivu A, Teresiak A, Scudino S, Calin M, Schultz L, Eckert J. Porous low modulus Ti40Nb compacts with electrodeposited hydroxyapatite coating for biomedical applications. Mat Sci Eng C. 2013;33:2280–7.

23. Xue W, Krishna BV, Bandyopadhyay A, Bose S. Processing and biocompatibility evaluation of laser processed porous titanium. Acta Biomater. 2007;3:1007–18.

24. Karageorgiou V, Kaplan D. Porosity of 3D biomaterial scaffolds and osteogenesis. Biomaterials. 2005;26:5474–91.

25. Wen C, Yamada Y, Hodgson P. Fabrication of novel TiZr alloy foams for biomedical applications. Mat Sci Eng C. 2006;26:1439–44.

26. Xing LQ, Ochin P. Bulk glass formation in the Zr–Ti–Al–Cu–Ni system. J Mater Sci Lett. 1997;16:1277–80.

27. Suryanarayana C, Inoue A. Bulk metallic glasses. Boca Raton, FL: CRC Press; 2011.

28. Scott MG. Crystallization in Amorphous Metallic Alloys. London: Butterworth & Co Publishers Ltd.; 1983.

29. Yu J, Jing T, Yang J, Li Q. Determination of activation energy for crystallizations in Ni–Sn–P amorphous alloys. J Mater Process Tech. 2009;209:14–7.

30. Srivastava AP, Srivastava D, Mazumdar B, Dey GK. Thermo-analytical study of crystallization process in metallic glass of Co69Fe3Si18B10. J Therm Anal Calorim. 2015;119:1353–61.

31. Wu J, Pan Y, Pi J. On non-isothermal kinetics of two Cu-based bulk metallic glasses. J Therm Anal Calorim. 2014;115:267–74.

32. Strbac G, Strbac D, Lukic-Petrovic S, Siljegovic M. Thermal characterization of glasses from Fe–Sb–S–I system. J Therm Anal Calorim. 2016;. doi:10.1007/s10973-016-5382-1.

33. Svoboda R, Malek J. Amorphous-to-crystalline transition in Te-doped Ge2Sb2Se5 glass. J Therm Anal Calorim. 2014;117:1073–83.

34. Svoboda R, Malek J. Is the original Kissinger equation obsolete today? J Therm Anal Calorim. 2014;115:1961–7.

35. Wei HD, Bao QH, Wang CX, Zhang WS, Yuan ZZ, Chen XD. Crystallization kinetics of (Ni0.75Fe0.25)78Si10B12 amorphous alloy. J Non-Cryst Solids. 2008;354:1876–82.

36. Zhang J, Wang W, Ma H, Li G, Lia R, Zhang Z. Isochronal and isothermal crystallization kinetics of amorphous Fe-based alloys. Thermochim Acta. 2010;505:41–6.

37. Nicoara M, Raduta A, Parthiban R, Locovei C, Eckert J, Stoica M. Low Young's modulus Ti-based porous bulk glassy alloy without cytotoxic elements. Acta Biomater. 2016;. doi:10.1016/j.actbio.2016.03.020.

38. Zhu SL, Wang XM, Qin FX, Yoshimura M, Inoue A. New TiZrCuPd quaternary bulk glassy alloys with potential of biomedical applications. Mater Trans. 2007;48(9):2445–8.

39. Khalifa HE, Vecchio KS. Thermal stability and crystallization phenomena of low cost Ti-based bulk metallic glass. J Non-Cryst Solids. 2011;357:3393–8.

40. Pratap A, Rao TLS, Lad KN, Dhurandhar HD. Kinetics of crystallization of titanium based binary and ternary amorphous alloys. J Non-Cryst Solids. 2007;353:2346–9.

41. Kasyap S, Patel AT, Pratap A. Crystallization kinetics of Ti20Zr20Cu60 metallic glass by isoconversional methods using modulated differential scanning calorimetry. J Therm Anal Calorim. 2014;. doi:10.1007/s10973-014-3753-z.

42. Lu XC, Li HY. Kinetics of non-isothermal crystallization in Cu50Zr43Al7 and (Cu50Zr43Al7)95Be5 metallic glasses. J Therm Anal Calorim. 2014;115:1089–97.

43. Huang Y, Shen J, Sun J, Yu X. A new Ti–Zr–Hf–Cu–Ni–Si–Sn bulk amorphous alloy with high glass-forming ability. J Alloy Compd. 2007;427(1–2):171–5.

44. Xia MX, Ma CL, Zheng HX, Li JG. Preparation and crystallization of Ti53Cu27Ni12Zr3Al7Si3B1 bulk metallic glass with wide supercooled liquid region. Mat Sci Eng A. 2005;390:372–5.

45. Xia MX, Zheng HX, Jian L, Ma CL, Li JG. Thermal stability and glass-forming ability of new Ti-based bulk metallic glasses. J Non-Cryst Solids. 2005;351:3747–51.

46. Gong P, Wang X, Yao K. Effects of alloying elements on crystallization kinetics of Ti–Zr–Be bulk metallic glass. J Mater Sci. 2016;51:5321–9.

47. Gong P, Yao K, Zhao S. Cu-alloying effect on crystallization kinetics of Ti41Zr25Be28Fe6 bulk metallic glass. J Therm Anal Calorim. 2015;121:697–704.

48. Kishimura H, Matsumoto H. Fabrication of Ti–Cu–Ni–Al amorphous alloys by mechanical alloying and mechanical milling. J Alloy Compd. 2011;509:4386–9.

49. Yanxin Z, Deqian Z, Yong ZWW, Mingxiang P. Kinetics of glass transition and crystallization of multicomponent bulk amorphous alloys. Sci China Ser A. 2000;43(11):1195–201.

50. Prajapati SR, Kasyap SA, Patel T, Pratap A. Non-isothermal crystallization kinetics of Zr52Cu18Ni14Al10Ti6. J Therm Anal Calorim. 2016;. doi:10.1007/s10973-015-4979-0.

51. Stoica M, Li R, Yavari AR, Vaughan G, Eckert J, Van Steenberge N, Romera DR. Thermal stability and magnetic properties of FeCoBSiNb bulk metallic glasses. J Alloy Compd. 2010;504:123–8.